



Semantic-aware structure-preserving median morpho-filtering

Kunal Pradhan¹ · Swarnajyoti Patra¹

Accepted: 2 February 2023

© The Author(s), under exclusive licence to Springer-Verlag GmbH Germany, part of Springer Nature 2023

Abstract

According to the recent developments, the most challenging part of texture filtering is to filter out the irregular and varying scale texture while preserving the structural contents with minimum distortion. For better handling varying scale irregular textural patterns, here we propose a semantic-aware structure-preserving filtering technique. Our technique, first, generates an edge-map by using semantic information extracted from the global and local morphological gradient histograms. Then using the generated edge-map, an adaptive median morpho-filtering is proposed by defining a dynamic window that avoids overlapping of textural and structural contents of the image. The experimental results for a variety of images show the potentiality of the proposed technique compared to the several state-of-the-art methods.

Keywords Morphological filters · Median filter · Texture smoothing · Structure-preserving filtering

1 Introduction

Natural images typically contain meaningful or significant (structure), as well as irrelevant or insignificant (texture) visual information. Structure-preserving image filtering is a key operation to extract the meaningful information from the images, which have a variety of applications in different fields like medical imaging, document analysis, remote sensing image analysis, etc [4,20,23]. Recent research focuses on the development of techniques which identify semantically significant objects from regular or irregular textural patterns for filtering. In the literature, such techniques that incorporate semantic information for automatic structure-texture separation is termed as semantic-aware or semantic filtering [8,45,51,53,54]. Over the last two decades, several edge-aware or edge-preserving filters such as bilateral filter [14,35,42,56,59], anisotropic diffusion [30,32], guided filter [17,55], weighted least square filter [12,46] have been developed and applied for different applications. For all these nonlinear filters, structure-texture separation is performed based on the measurement of local contrast or gradients, where the structural edges are identified as the pixels having relatively high gradients and fine-scale details are as the textures. These filtering techniques integrate prior edge infor-

mation within the smoothing operations aiming to extract or remove certain image details. Thus, they fail when the images have high gradient textural contents that can be confused with the structural edges.

In order to overcome this limitation, several optimization-based filtering approaches have been proposed in the literature by considering the first like L0 gradient minimization [8,40] or second order gradients [11,31], Total Variation (TV) [34,38], Relative Total Variation (RTV) [49]. They explored spatial relationship, frequency and symmetry of local distribution as textural measures. Some techniques introduced patch-based statistical descriptors like region co-variance [21] or modified RTV [9] as a texture descriptor. As the patch-based approaches used fixed size patches (windows) to calculate textural descriptors, it is often seen that the structural regions are also included by these patches, which makes them less effective. To mitigate this problem, some edge-aware fixed shape patch shifting strategies or dynamic shape patch-based filtering are proposed in [9,25]. Since the edges are not always horizontal or vertical or diagonal aligned, only shifting of fixed shape patches does not solve the problem. Considering linearity of the edges, edge aligned dynamic shape patches may solve this problem. In later developments, several techniques are proposed in this direction [19,50,51,55], where some edge-aware measures are used to design dynamic shape patches. The main problem of these methods is that they required a proper edge-map

✉ Swarnajyoti Patra
swpatra@tezu.ernet.in

¹ Department of Computer Science and Engineering, Tezpur University, Napam, Assam 784028, India

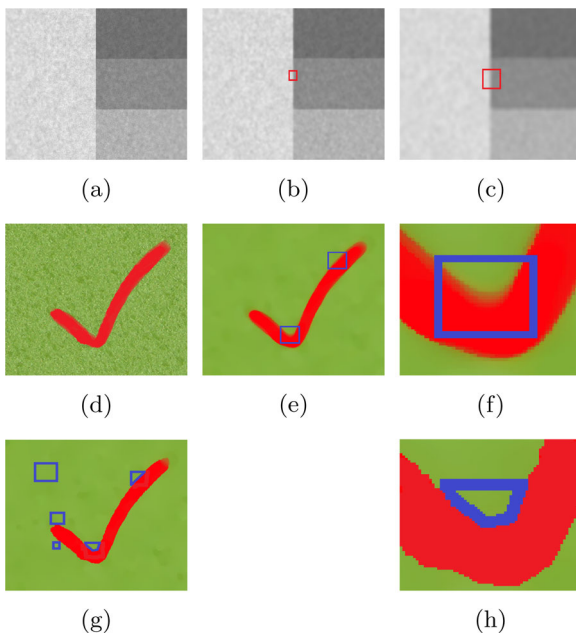


Fig. 1 **a** Original image with simple structure. **b, c** The filter images obtained using smaller and larger static box windows. **d** Original image with complex structure. The filter images and their zoomed portion obtained using **e, f** static box window, and **g, h** proposed dynamic window

as prior information and the generation of such an edge-map is a challenging task.

In this article, we have proposed a semantic-aware robust structure-preserving filtering technique. Our technique defines a novel method to obtain an edge-aware adaptive window of dynamic shape for filtering each pixel of the image by excluding its neighbor pixels belonging to different textural or structural regions. Figure 1 illustrates the importance of the uses of adaptive dynamic shape windows in comparison to fixed shape windows for filtering. As shown in Fig. 1b, the small fixed shape window does not work well to filter out the large-scale textures. On the other hand, the large window does not preserve edges properly(blur the edges) as shown in Fig. 1c, f. Since larger windows are useful to identify large-scale textures and smaller ones are effective for both detection and preservation of smaller structural edges. Defining an appropriate dynamic window for filtering varying size textures or structures is very much important. In the proposed work this issue is addressed by defining edge-aware adaptive dynamic shape windows as shown in Fig. 1g, h. In our technique, first, a novel method is proposed to generate the semantic edge-map by computing the skewness of global and local morphological gradient histograms. Then, using the generated edge-map an edge-aware structure-preserving adaptive median morpho-filter is designed. The edge-map generation followed by median morpho-filtering iteratively runs to generate the final filter image. Note that morphological filters generally preserve the

larger structural shapes while removing the smaller irregular shapes. In contrast, median filter converges the pixel values into the background pixels with greater counts. Thus, the proposed median morpho-filter merges the narrow texture to its original background as well as preserves the significant structures. The experimental results show that unlike most of the existing techniques, our filtering can achieve multiple conflicting goals, like identifying and removing texture, preserving structural edges, protecting easy-to-miss features such as corners, and preventing over-sharpening and/or over-blurring artifacts/distortions. The main contributions of this work are:

- Proposes a texture-structure decomposition technique by analysing the morphological gradient histogram of the image.
- Proposes a semantic-aware median morpho-filter for texture smoothing while preserving the significant structures.

The rest of the paper, Sect. 2 presents related works. Section 3 gives a brief introduction of morphological and median filters. The details of the proposed technique are presented in Sect. 4. Experimental results are discussed in Sect. 5 and finally, Sect. 6 provides conclusion of this work.

2 Background and literature review

Image filtering is an essential operation with a variety of applications in computational photography and image analysis. Such an operation decomposes an image into the prominent structure and fine-scale detail making it easier for subsequent image manipulation like tone mapping, detail enhancement, visual abstraction, scene understanding, etc. The large number of filtering methods proposed in the literature are mainly four categories: average based [17,53], optimization based [7,46,48,49], rank order based [3,29] and patch based [9,21,41]. The filtering methods in the first two are particularly effective for removing noises and fine-scale geometric details. For example, bilateral filter [2,42], weighted least square filter [12,27,46], L0 smoothing [40,48], and the methods using anisotropic diffusion [30,32,52] are successfully used to filter low-contrast noise but failed for smoothing high-contrast noises or textures. Rank order-based filtering techniques are capable of filtering high-contrast noises or textures using local histogram where the color/intensity of each pixel is replaced by some order ranked value (like maximum, minimum, median, etc) of the neighboring pixels. Thus, they preserve the original contrast in the filtered image. Texture filtering [26,39,58] is all about removing the insignificant regular or irregular patterns (textures) from the filtered image while preserv-

ing the significant structures or objects of the image. Since the measure of the visual patterns of regular or irregular textures is not considered by the filtering methods of the first three categories, they are not that effective in texture filtering. Whereas, patch-based filters are capable of considering the measurements of visual patterns. Thus, more suitable for texture filtering. Generally, visual patterns are measured with axis-aligned patches or by computing the patch-based statistical measures. There are patch-based techniques presented in [5,6] performed filtering by applying some non-local measurements, but the textural measurements are not taken into consideration. As a result, these methods are less effective for texture filtering. The spatial relationship, frequency, and symmetry/asymmetry of the textural pattern of regular or near-regular shapes are taken into consideration for texture identification and filtering is presented in [16,28]. However, for developing a robust texture filtering technique, filtering out arbitrary textures of both regular or irregular shapes/patterns is important. Though, finding out the insignificant irregular textures and removing them in a semantical sense is always a challenging task. In this regard, Rudin et al. [34] have effectively enforced total variation (TV) regularization constraints to preserve large-scale edges. In order to further improve the texture-structure separation based on TV, Xu et al. [49] introduced relative total variation (RTV). Both the methods are developed based on the concept of the aggregation of signed gradient values within a local window/patch often produces a larger absolute value for structural edges than its textural counterpart. As the texture regions usually produce inconsistent gradients within a local window, the gradient measure is used to differentiate textural and structural edges. However, such a measure may misidentify small structural edges as textures. Moreover, the use of larger neighboring windows overlapping different regions may result in very similar RTV values for neighboring pixels of different regions. As a result, these methods are prone to produce over-smooth structural edges. In [21], Karacan et al. introduced region co-variance descriptor as textural measurement that uses second-order statistics extracted from the fixed size patches. Although, this descriptor performs better separation between texture and structure, but fails to avoid the over blur effect at the structural edges as the overlap patches near an edge always share almost similar region co-variances.

To mitigate this problem, some recent techniques have tried to optimize the position of patches [9] or the size of patches [55]. For computing the textural measure, Cho et al. [9] assumed that a pixel may not be always well represented by the patch centered on it. Finding out the nearby patch which is least likely to contain structural edges can resolve the patches overlapping issue. Thus, they have proposed patch shifting technique to avoid the neighboring windows over-

lapping problem, which has improved the effectiveness of the textural measures. The main challenge in this technique is to choose an effective patch size and its position. In [24], to avoid over blurring smaller structural edges problem, a smaller patch (shrink version of the original patch) is considered for the pixels located at the nearby structural edges, while a larger patch (original patch) is used for the pixels representing the texture regions. Since the technique is only able to shrink the original patches and unable to expand them, it prevents the original patches from being as large as needed. So, filtering of large-scale textures is not efficiently done by this method. For multiple scaled texture smoothing, a scale-aware method is presented in [19]. Depending on the patch-based statistics this method finds an optimal per-pixel adaptive smoothing scale for texture filtering. It used RTV-based statistics for the textural measure. Because of the over-blurring issue with RTV, this method may fail to estimate the scales of textures properly. As a result, large-scale texture filtering may not be efficiently performed by this method. As the scale of the textures is related to the gradients, Lee et al. [22] proposed an adaptive gradient smoothing method by introducing the interval gradient measure. Since the estimation of the scales of textures depends on the statistics of gradients, the method is effective when the scale of the textures are similar. The textures with large varying texels are not properly handled by this method as the statistics of gradients also change drastically. So, the main challenges for developing a robust structure-preserving filtering technique lies in the fact of handling varying scales of textural patterns.

To address this some recent developments proposed dynamic shape adaptive window generation by taking into consideration of the linear characteristic of the structural edges [25,29,50]. They approximate the linearity of the structural edges by local gradient directions. As the structural edges are not always axis-aligned, approximating the linearity of edges locally is not an easy task. There are some researches directed toward the development of edge-aware or semantic-aware filters [8,13,53,54,57,60]. Some of these methods define edge-aware adaptive window for filtering depending on a prior edge-map generated by introducing modified edge features or using existing edge detection techniques. As the generation of a proper edge-map is a challenging and developing task, semantic-aware filtering has taken more exploration in recent research.

3 Morphological and median filters

Our filtering technique exploits the properties of morphological and median filters [15,37]. This section provides a brief description of these two filtering techniques.

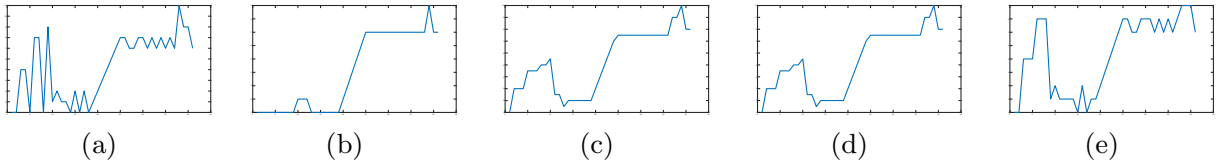


Fig. 2 **a** Original 1-dimensional signal and the corresponding filtered signal obtained by applying **b** Opening, **c** Closing, **d** (Opening + Closing)/2, and **e** Median operations with a fixed SE of size 3 unit

3.1 Morphological filter

It works on the rank ordering principle. The basic two operations dilation (δ) and erosion (ε) filter the image by replacing the center pixel of the predefined neighbor called structuring element (SE) with the local maximum and minimum value, respectively. The other operations such as opening ($\delta(\varepsilon)$) and closing ($\varepsilon(\delta)$) are designed by applying successive alternative operations of dilation and erosion. The very basic nature of these operations intuitively removes the impulse noises smaller in size than the neighboring window (i.e. SE) without affecting the basic shape of the objects. Figure 2 shows the filtering results obtained on a 1-dimensional signal by applying different morphological operations with a fixed SE of size 3 unit. In the proposed technique morphological filter is exploited to improve the discrimination between structural edges and textural regions of the image.

3.2 Median filter

It is a popular rank order filter that replaces each pixel by the median value of the defined neighboring pixels. As the median value always divides the distribution into equal two parts in the same number of counts, it is naturally not sensitive to the impulse noise/outliers. Unlike the weighted average filters, median filter always replaces the pixel value with an existing value within the window if the number of pixels in the window is odd. If the neighbor pixels follow a positively skewed distribution then the median will be less than the mean. On the other hand, for a negatively skewed distribution the median will be greater than the mean. For a symmetric/near-symmetric distribution (i.e., skewness is near to zero) the median will be equal to or closer to the mean value. Figure 2e shows the filtering result obtained from Fig. 2a by applying median operation with a fixed window of size 3 unit. The median filter merges the high intensity textures to its low intensity background if the local distribution is positively skewed and the low intensity texture to its high intensity foreground if the distribution is negatively skewed. In our proposed method, this intuitive property of the median filter is exploited to develop a robust edge-preserving smoothing technique.

4 Proposed technique

The proposed filtering technique has two main tasks. First, it generates a binary edge-map by analysing the morphological gradient histogram of the image. Then, based on the generated edge-map, a semantic edge-aware median morpho-filtering technique is proposed to generate the filtered image. The detailed steps of the proposed filtering technique are presented in the following subsections:

4.1 Generation of gradient image

Our filtering method works on both gray scale as well as colour images. If the input is a colour image, then its corresponding gray scale image is used to generate the morphological gradient image. In many cases, the images may have high gradient textural contents which can be confused with the structural edges. In order to improve the discrimination between textural and structural contents of the image, in this work, we proposed a pre-processing step that performs filtering on the input image by defining a morphological filter combining opening and closing operations. Let I_{gray} be the gray scale image obtained from the input image. The proposed pre-processing step generates a filtered image J from I_{gray} as follows:

$$J = (\delta_{\text{SE}}(\varepsilon_{\text{SE}}(I_{\text{gray}}) + \varepsilon_{\text{SE}}(\delta_{\text{SE}}(I_{\text{gray}})))/2 \quad (1)$$

Figure 2a shows a 1-dimensional signal with some high textural oscillations having equal or higher gradients than the structural edges. Figure 2d shows the filtered signal obtained by applying the morphological operation define in (1). From this figure, one can see that the average of opening and closing removes the lower textural oscillations and diminishes the higher textural gradient while keeping the higher structural gradients mostly unchanged. Thus, it helps to create a difference between high gradient textural and structural contents in the gradient domain. To better understand the usefulness of the morphological operation defined in (1), Fig. 3 shows a real image and the filtered images obtained by applying different morphological operations. It also plots the intensity values of the pixels on the red line (passes through both textural and structural regions) for these images. From Fig. 3a it is seen that in the original image, there are some textural

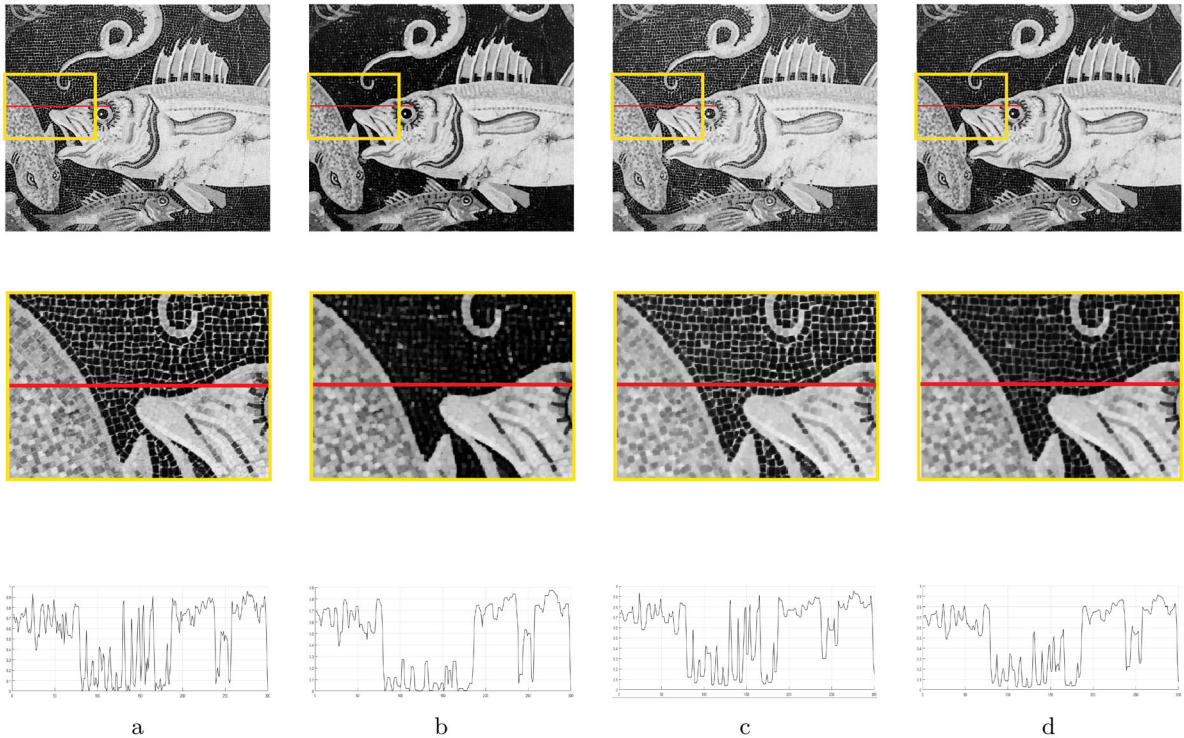


Fig. 3 **a** Original image, its zoomed image of the area enclosed with yellow rectangle and the intensity values of the pixels on the red line. The filtering results obtained by applying **b** Opening, **c** Closing, and **d** (Opening+Closing)/2

edges whose gradients are as high as the structural edges. From Fig. 3b, c one can see that the individual operation of the opening increases the darker textural gradient and closing increases the brighter textural gradient. But the average of both the operations as defined in (1) diminishes the textural high gradients (or impulse noises) while keeping structural edges with minimum distortion as shown in Fig. 3d. After obtaining the filtered image J , the proposed technique generates morphological gradient image J_{mg} as follows [33]:

$$J_{mg} = (\delta_{SE}(J) - \varepsilon_{SE}(J)) \quad (2)$$

Figure 4a, b is the gradient image obtained without and with applying the pre-processing step, respectively. From these figures, one can see that the proposed pre-processing step diminishes high gradient textures while keeping the structural edges with minimum distortions.

4.2 Generation of edge-map

The gradient image J_{mg} obtained from (2) is used to generate the edge-map. For an image, a very less number of pixels are associated with significant structural edges as compared to the non-edge pixels. Thus, in the gradient image J_{mg} , higher gradient pixels associated with the structural edges are much lesser in number than the lower gradient pixels associated with smooth areas. So, the histogram of the gradi-

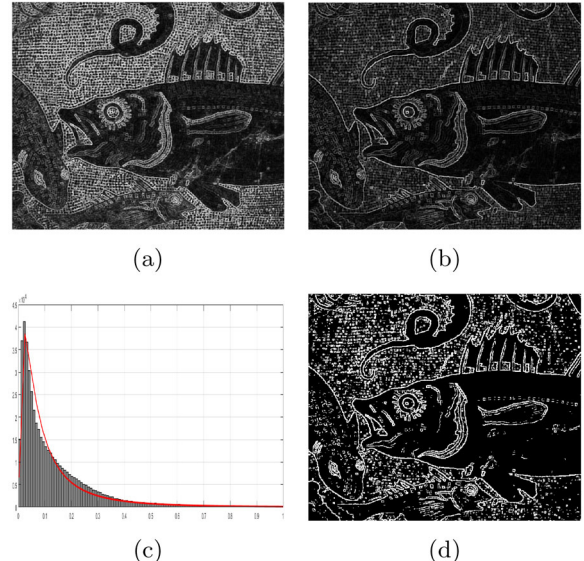


Fig. 4 **a** Gradient image without applying pre-processing, **b** gradient image with applying proposed pre-processing and **c** its histogram with the best fitted log-normal distribution curve by maximum likelihood estimator. **d** The initial edge-map E_b obtained by applying global threshold t_1

ent image is likely to follow a positively-skewed distribution with a high peak of lower values and a right-tail of higher values, as shown in Fig. 4c. Note that the domain of the gra-

gradient image J_{mg} is associated with non-negative values. So the positively-skewed histogram of the non-negative gradient can be assumed to follow a log-normal distribution [1,10]:

$$\begin{cases} f(x) = \frac{1}{x\sigma\sqrt{2\pi}} e^{-\frac{(\ln(x)-\mu)^2}{2\sigma^2}} & \text{where } x > 0, \sigma > 0 \\ \mu = \ln\left(\frac{v}{\sqrt{1+\frac{\gamma^2}{v^2}}}\right) \\ \sigma = \sqrt{\ln\left(1 + \frac{\gamma^2}{v^2}\right)} \end{cases} \quad (3)$$

The probability density function of a log-normal distribution $f(x)$ for a random variable x is a continuous distribution of positive values as defined in (3), such that the logarithm of x i.e., $\ln(x)$ follows a normal distribution $N(\mu, \sigma)$. Where $\mu = \ln(m)$ is the scale parameter represents mean of $\ln(x)$ and m is the median of the x , σ is the shape parameter represents standard deviation of $\ln(x)$. The standard deviation and mean of x are denoted as γ and v respectively. Since the gradient image J_{mg} may have zero gradient value we have added a very small positive value η as $J_{mg} = J_{mg} + \eta$ to model J_{mg} as log-normal distribution. In order to generate an accurate edge-map, first, a global threshold t_1 from the histogram of the gradient image J_{mg} is detected by exploiting the properties of the log-normal distribution. The threshold t_1 roughly differentiates the edge and non-edge pixels in the gradient image. For a log-normal variate x , the corresponding normal distribution $\ln(x)$ contains 66.68% of values within the range $(\mu - \sigma, \mu + \sigma)$, which corresponds to the high peak portion $(e^{\mu-\sigma}, e^{\mu+\sigma})$ of the log-normal distribution. The right-tail portion ($\geq e^{\mu+\sigma}$) of the corresponding log-normal distribution contains less than 33.32% of total values. In this work, we have taken the global threshold $t_1 = e^{\mu+\sigma}$ to roughly differentiate between the edge (high gradient) and the non-edge (low gradient) pixels. After obtaining the threshold t_1 , the initial binary edge-map E_b from the gradient image is generated as follows:

$$E_b(p) = \begin{cases} 1, & \text{if } J_{mg}(p) \geq t_1 \\ 0, & \text{if } J_{mg}(p) < t_1 \end{cases} \quad (4)$$

The initial edge-map E_b generated by considering the global threshold t_1 may have textural edges along with structural edges. To further reduce the presence of non-structural edges in the edge-map, proposing a novel technique to refine it. For each edge pixel p in E_b , the proposed technique constructs a local histogram $H(J_{mg}^W)$ of the gradient image J_{mg} considering a fixed size window $W = (w \times w)$ centering at pixel p . Then to determine whether the pixel p belongs to a structural edge or not, it computes the non-parametric

skewness value Sk_p from the histogram $H(J_{mg}^W)$ as follows:

$$\begin{cases} Sk_p = \frac{\mu_1 - m_1}{\sigma_1} \\ \mu_1 = \text{mean of } H(J_{mg}^W) \\ m_1 = \text{median of } H(J_{mg}^W) \\ \sigma_1 = \text{standard deviation of } H(J_{mg}^W) \end{cases} \quad (5)$$

In the proposed technique for each edge pixel p in J_{mg} , if the skewness Sk_p is positive, then the pixel remains an edge pixel. Otherwise, it converts into a non-edge pixel. So, the proposed technique generates the refine edge-map E_r from the initial edge-map E_b as follows:

$$E_r(p) = \begin{cases} 1, & \text{if } E_b(p) = 1 \text{ and } Sk_p > 0 \\ 0, & \text{Otherwise} \end{cases} \quad (6)$$

Figure 5 show the initial edge-map E_b and the corresponding refined edge-map E_r produced by the proposed technique for two different images. In order to better understand how the local skewness value of the gradient image helps to find whether a pixel is an edge pixel or not, five edge pixels p_1, p_2, p_3, p_4 , and p_5 from different portions of the gradient image J_{mg} obtained from Fig. 6a are chosen. Considering these pixels as center pixels, the corresponding portions in the original image covered by the local windows (red boxes) are shown in Fig. 6a. The zoomed version of these windows are shown in Fig. 6c–g. From these figures, one can see that pixels p_1 and p_3 originally belong to the structural-edge regions, whereas pixels p_2, p_4 and p_5 originally belong to the textural or smoother regions. Figure 6h–l shows the local histogram (considering window W) of the gradient image J_{mg} associated to the center pixel p_1, p_2, p_3, p_4 and p_5 respectively. From these figures, it is seen that the gradient distribution of the local histograms corresponding to the pixels p_1 and p_3 which are on the structural-edge regions are positively skewed (i.e., their local histograms from J_{mg} contain few locally higher gradient pixels those are part of the significant edges). Whereas, the distribution of the local histograms corresponding to the pixels p_2, p_4 and p_5 which belong to the textural or smoother regions are not positively skewed (i.e., their local histograms in J_{mg} contain more locally higher gradient pixels or similar gradient pixels those are part of some textural or smoother regions). Table 1 reports the skewness values computed for these five local histograms. Form the table, one can see that the pixels having positive skewness values are on the structural-edges, and pixels of negative skewness are on the textural/smooth regions. Note that for the presence of high gradient noises some pixels in the textural region may possess positive skewness values. In such cases, our method may wrongly identify these pixels as structural-edge pixels. To mitigate this, in the proposed work

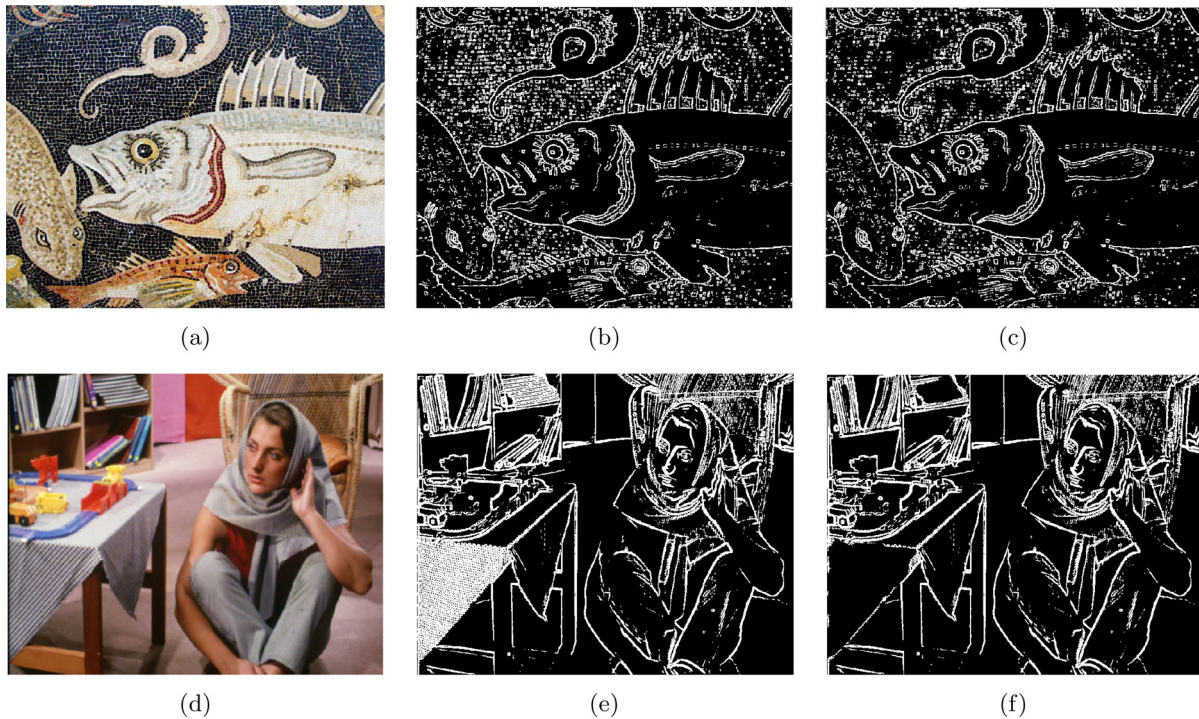


Fig. 5 **a, d** Original images, their **b, e** initial edge-maps E_b , and **c, f** refined edge-maps E_r produced by the proposed technique

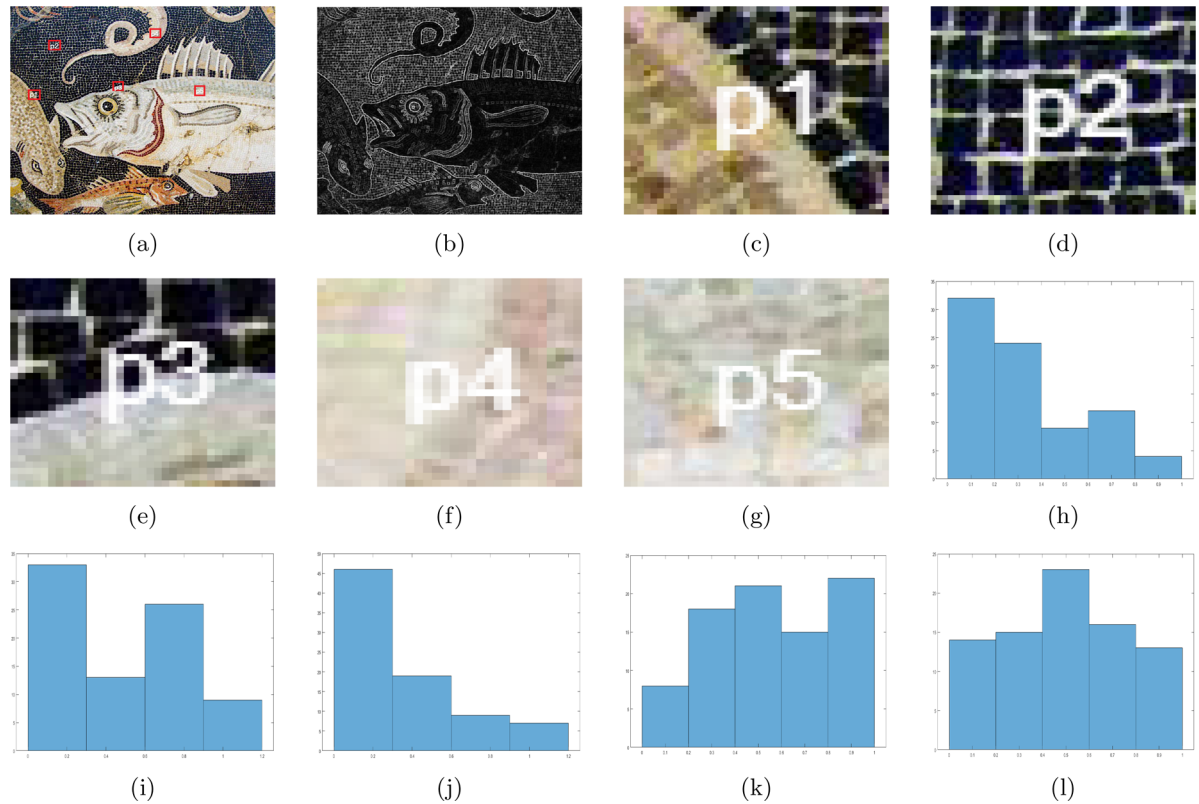


Fig. 6 **a** Original image I and **b** the corresponding gradient image J_{mg} . **c, d, e, f, g** The zoomed version of the red windows of centre pixels p_1, p_2, p_3, p_4 and p_5 are shown in the original image and **h, i, j, k, l** their corresponding local histograms obtained from the gradient image

Table 1 The skewness values obtained from local histograms associated to the different pixels of the gradient image

Test pixels (p)	Skewness(Sk_p)	Status
p_1	1.0715	Edge
p_2	-0.0083	Non-edge
p_3	0.7069	Edge
p_4	-0.0467	Non-edge
p_5	-0.0733	Non-edge

the edge-map for the next iteration is updated based on the filtered image generated in the current iteration.

4.3 Median morpho-filtering

In order to produce the filter image, we propose a novel semantic-aware structure-preserving filtering technique by exploiting the generated edge-map E_r . Let I be the original image to be filtered and E_r be the corresponding edge-map generated by the proposed technique. By exploiting the edge-map E_r , our technique follows different approaches to determine dynamic window of the median filter for filtering the edge and non-edge pixels of the image. For filtering the pixels belong to textural regions (i.e., non-edge pixels), our technique determines the dynamic size square window by looking into the surrounding edge pixels present in E_r . For each non-edge pixel, the algorithm starts with a small square window L_w and then increases its size uniformly until a sufficiently large size square window is obtained or an edge pixel is found. Thus, for filtering non-edge pixels our algorithm determine dynamic size square windows by looking into the edge pixel on the edge-map. The blue boxes in Fig. 7 depicts the windows obtained by the proposed algorithm for some non-edge pixels. From this figure one can see that the larger size windows are formed for filtering the pixels of textural areas which are far from the structural-edges and smaller size windows are formed for filtering the pixels near to the structural-edges. Thus, the size of the windows defined by the proposed algorithm for filtering non-edge pixels are adaptive in nature. On the other hand, for filtering the pixels belong to structural-edges (i.e., edge pixels), our technique determines shape of the window of median filter dynamically by identifying the appropriate object in which the edge pixel belongs. Note that edge pixels are always belong to either one of the two objects which are responsible to form the edge. By computing the intensity value of the edge pixel within a fixed size window our algorithm tried to find out the appropriate object in which the considered edge pixel belongs and then reshape the window for filtering. The red curves in Fig. 7 formed the dynamic windows by considering appropriate edge pixel for filtering some structural-edge pixels. The size of the windows

defined by the proposed algorithm for filtering edge pixels are also adaptive in nature.

In greater detail, let p be an edge pixel and its intensity value in the original image I is I_p . Our algorithm first defines a fixed size square window W_s by using p as a center pixel. Considering the window W_s , let I_{W_s} and $E_r^{W_s}$ be the sub-image obtained from the original image I and the edge-map image E_r , respectively. Let $I_{W_s}^e$ represents the intensity values of the edge pixels in I_{W_s} . The middle intensity value R_{mid} of the edge pixels within W_s will be $R_{mid} = (\max(I_{W_s}^e) + \min(I_{W_s}^e))/2$. The pixel intensity I_p is larger (or smaller) than R_{mid} implies that the edge pixel p belongs in the higher(or lower) intensity object. Thus, for filtering the pixel p , if I_p is larger than R_{mid} then the pixels in I_{W_s} having higher intensity values than R_{mid} are considered to define the window W_s^u of the median filter. Otherwise, the pixels in I_{W_s} having lower intensity values than R_{mid} are considered to define the window W_s^l of the median filter. In the proposed technique for filtering edge pixels the dynamic size window W_s^a of the median filter within W_s is defined as follows:

$$\begin{cases} R_{mid} = (\max(I_{W_s}^e) + \min(I_{W_s}^e))/2 \\ W_s^l = \text{pixels in } W_s \text{ for which } (I_{W_s} \leq R_{mid}) \\ W_s^u = \text{pixels in } W_s \text{ for which } (I_{W_s} \geq R_{mid}) \\ \text{if } (I_p \leq R_{mid}), \text{ then } W_s^a = W_s^l \\ \text{if } (I_p > R_{mid}), \text{ then } W_s^a = W_s^u \end{cases} \quad (7)$$

From the above equations, one can see that the dynamic window W_s^u is formed when the intensity of the center pixel (I_p) is greater than R_{mid} , otherwise it is formed the dynamic window W_s^l for filtering the edge pixel p . The proposed algorithm splits the fixed size window W_s to form an edge adaptive dynamic shape window along the approximate edge alignment. The red curves in Fig. 7 connected with appropriate edge pixels shows the dynamic windows defined by the proposed algorithm for filtering edge pixels. From this figure, one can see that windows at edge are formed according to the edge linearity. Since there is a possibility that the window division for edge pixels may not always be as accurate as the actual edge alignment. In such cases, a small amount of edge distortion may occur after applying the proposed adaptive median filter. In order to refine these distortions, the morphological operation defined in (1) with a small static window is applied. The adaptive median filtering followed by morphological filtering alternatively suppresses/refines the artifacts/distortions of each other. That is, the edge dilation of median filtering regains its sharpness by the morphological counterpart and the impulse edge shape distortion of morphological filtering is smoothed by median filtering. In this work, we refer this technique as adaptive median morpho-filtering.

All the steps of the proposed technique need to be repeated multiple times to generate the desire filter image. Let I_f be the filter image obtained from the input image I . Then the output image I_f is considered as the input image ($I = I_f$) for the next iteration. Figure 8 shows the edge-maps produced by the proposed technique at different iterations and the filter image obtained after 3rd iteration. Figure 9 shows the filter images produced by the proposed technique at different iterations. From these figures, it is seen that the proposed technique successfully preserves the structure of the objects. The proposed technique is summarized in Algorithm 1.

Algorithm 1 Proposed semantic-aware structure preserving filtering technique

```

1: Input: Image  $I$ 
2: Output: Filtered Image  $I_f$ 
3: Obtain gray scale image  $I_{gray}$  from the input image  $I$ 
4: Generate filter image  $J = (\delta_{SE}(\varepsilon_{SE}(I_{gray}) +$ 
 $\varepsilon_{SE}(\delta_{SE}(I_{gray}))/2$ 
5: Generate gradient image  $J_{mg} = \delta_{SE}(J) - \varepsilon_{SE}(J)$ 
6: for iteration = 1 to  $n_{itr}$ 
7:   for all pixel  $p \in J_{mg}$ 
8:     if  $(J_{mg}(p) \geq e^{(\mu+\sigma)})$ 
9:        $E_b(p) = 1$ 
10:    else
11:       $E_b(p) = 0$ 
12:    end if
13:   end for
14:   for all pixels  $p \in E_b$ 
15:     if  $(E_b(p) = 1 \wedge Sk_p > 0.0)$ 
16:        $E_r(p) = 1$ 
17:     else-if  $(E_b(p) = 1 \wedge Sk_p \leq 0.0)$ 
18:        $E_r(p) = 0$ 
19:     end if
20:   end for
21:   for image band  $c = 1$  to  $C$ 
22:     for all pixels  $p \in I_c$ 
23:       if  $(E_r(p) = 1 \wedge I_c(p) \leq R_{mid})$ 
24:         Define window  $W_s^a = W_s^l$  using (7)
25:       else-if  $(E_r(p) = 1 \wedge I_c(p) > R_{mid})$ 
26:         Define window  $W_s^a = W_s^u$  using (7)
27:       else-if  $(E_r(p) = 0)$ 
28:         Define window  $W_s^a$  by starting from  $L_w$ 
29:         to a maximal size square window that does
30:         not contain any edge content.
31:       end if
32:       Replace  $I_c(p)$  by the median value from  $I_c$ 
33:       within the window  $W_s^a$ .
34:     end for
35:    $I_f(c) = (\delta_{SE}(\varepsilon_{SE}(I_c) + \varepsilon_{SE}(\delta_{SE}(I_c)))/2$ 
36:   end for
37:    $I = I_f$ 
38: end for

```

5 Experimental results and analysis

In order to assess the potentiality of the proposed filtering technique, it compare with six popular state-of-the-art structure-preserving smoothing techniques such as bilateral texture filtering(BTF) [9], relativity of Gaussian(RoG) [7], scale-aware texture filtering(SATF) [19], structure adaptive total variation(SATV) [38], fast adaptive bilateral filtering(FABF) [14], and iterative least square(ILS) [27].For fair comparison the values of the parameters of all these state-of-the-art methods are chosen carefully. Whenever possible, the

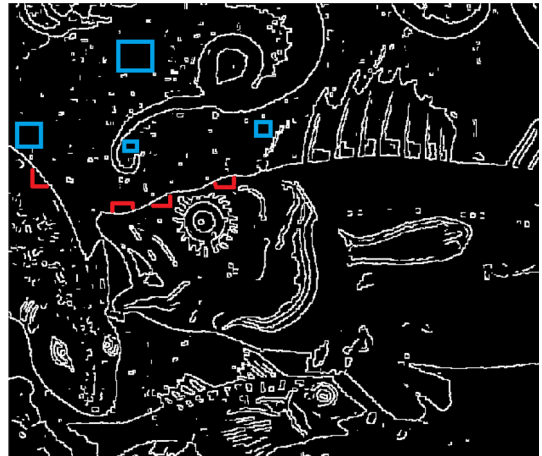


Fig. 7 Adaptive windows for median filter is designed using the generated edge-map (E_r)

values of the parameters are taken from the respective papers for which the best results are given. Otherwise, we have manually set the parameters values that provided best possible results using trial and error method. All the images used in this study are publicly available at <http://www.cse.cuhk.edu.hk/~leojia/projects/texturesep/index.html> and <http://cg.postech.ac.kr/publications>. The details of the comparisons are given in the following subsections.

5.1 Qualitative comparison

Qualitative comparison between the proposed and the state-of-the-art methods are performed on the basis of how much they are effective to differentiate texture and structure by smoothing out fine details of textures while preserving the significant structures. Figure 10 shows the filtering results obtained by the proposed as well as the six state-of-the-art methods for the part of the roman marine life mosaic image. By looking into the zoomed portions of the filter images produced by the different methods, it is seen that our method is outperforming than the existing methods in both the terms: i) texture smoothing and ii) structure preserving. From the figure, it is observed that BTF [9], SATF [19], FABF [14] are capable of preserving the significant structures but producing poor smoothing results for the varying scale textures. Whereas, the RoG [7] filtering technique is good in texture smoothing but fails to preserve the smaller structures and the ILS [27] produces blur structural objects. On the other hand, the proposed method is equally effective in smoothing of varying scales texture as well as preserving the significant structures of different sizes. Unlike the other methods, instead of blurring, the proposed method sharpens the filtered image by preserving the structural edges. Moreover, it capable to preserve the small structural details like the iris and eyelids of the fishes more prominently than the oth-

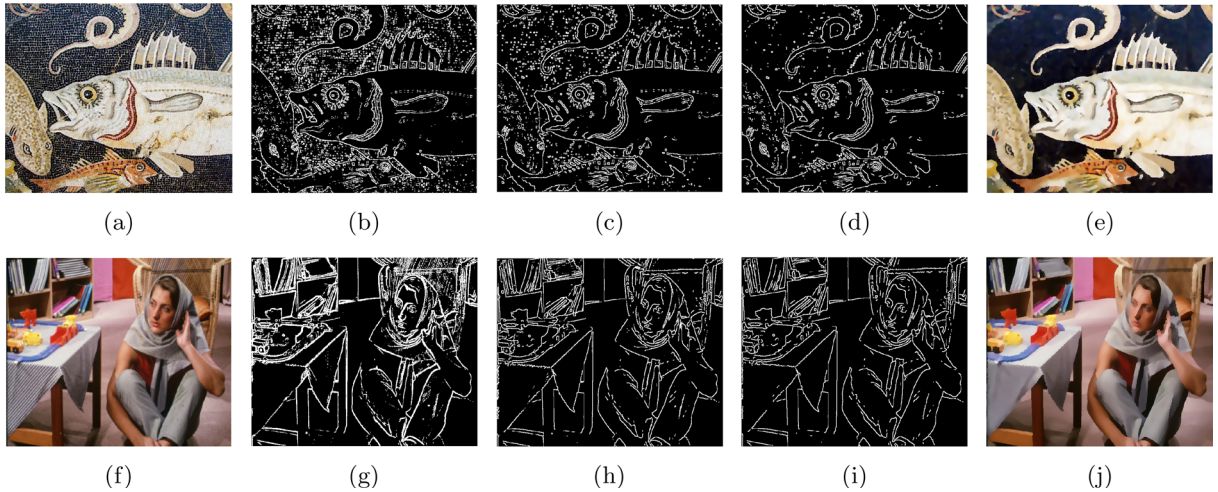


Fig. 8 **a, f** Original images and the generated edge-maps after **b, g** iteration 1, **c, h** iteration 2, **d, i** iteration 3. **e, j** Filter images produced by the proposed technique after 3rd iteration

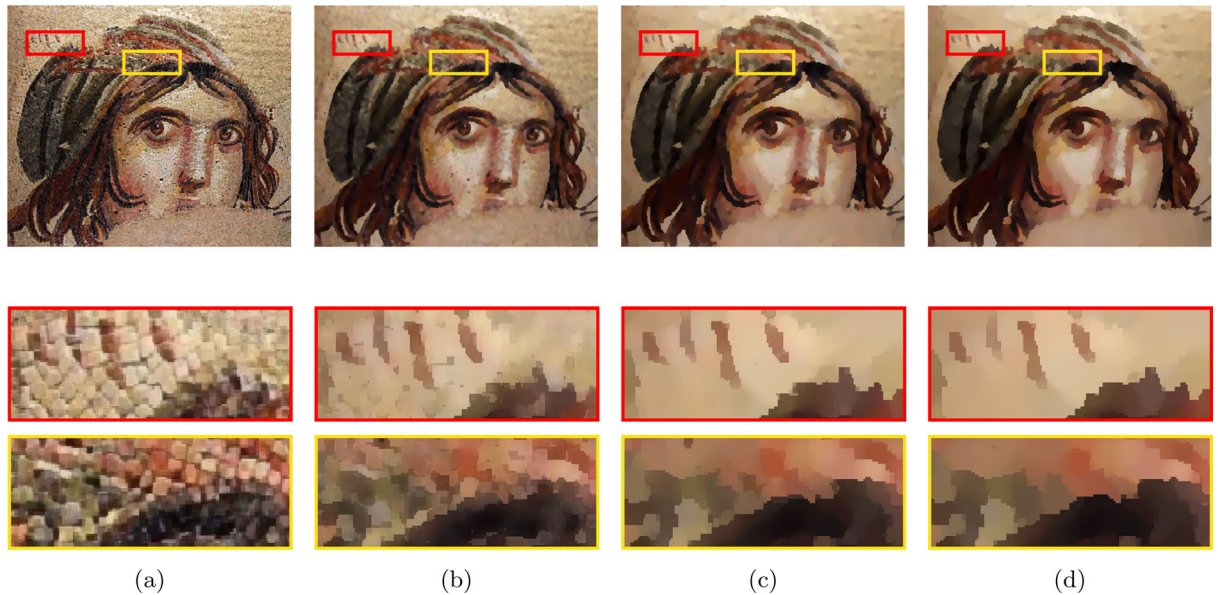


Fig. 9 **a** Original image and some zoomed portions of it. Filter images obtained by the proposed technique after **b** iteration 1, **c** iteration 3, and **d** iteration 5

ers. The experiment performed on a large number of images containing different type of textural patterns the proposed technique always produced satisfactory results. The filtering results obtained from few of such images are shown in Figs. 11, 12, and 13. From these figures one can see that for the input images of smaller textural patterns, e.g., part of the roman still life mosaic image in Fig. 11a as well as the images of larger texels, e.g., the brick wall graffiti image in Fig. 12a, the proposed method always provides better or as good as the best result produced by the existing state-of-the-art methods. Looking into the filtering results in Fig. 11 and Fig. 12, one can see that our method outperforms than most of the existing techniques. Figure 13 shows the filter-

ing results of the proposed technique on few more popular images containing rich textural variation. In order to further assess the effectiveness of our filtering technique, we have added an artificial grid texture and Gaussian noise (mean = 0, variance = 0.01) to the original Lena image and then applied our filtering technique to restore it. Figure 14 shows the original image, images after adding artificial texture and noise, and the filtered image generated by the proposed technique. By analysing these results we can claim that our filtering technique is able to achieve multiple conflicting goals, like identifying and removing texture, preserving structural edges, protecting easy-to-miss features such as corners, and

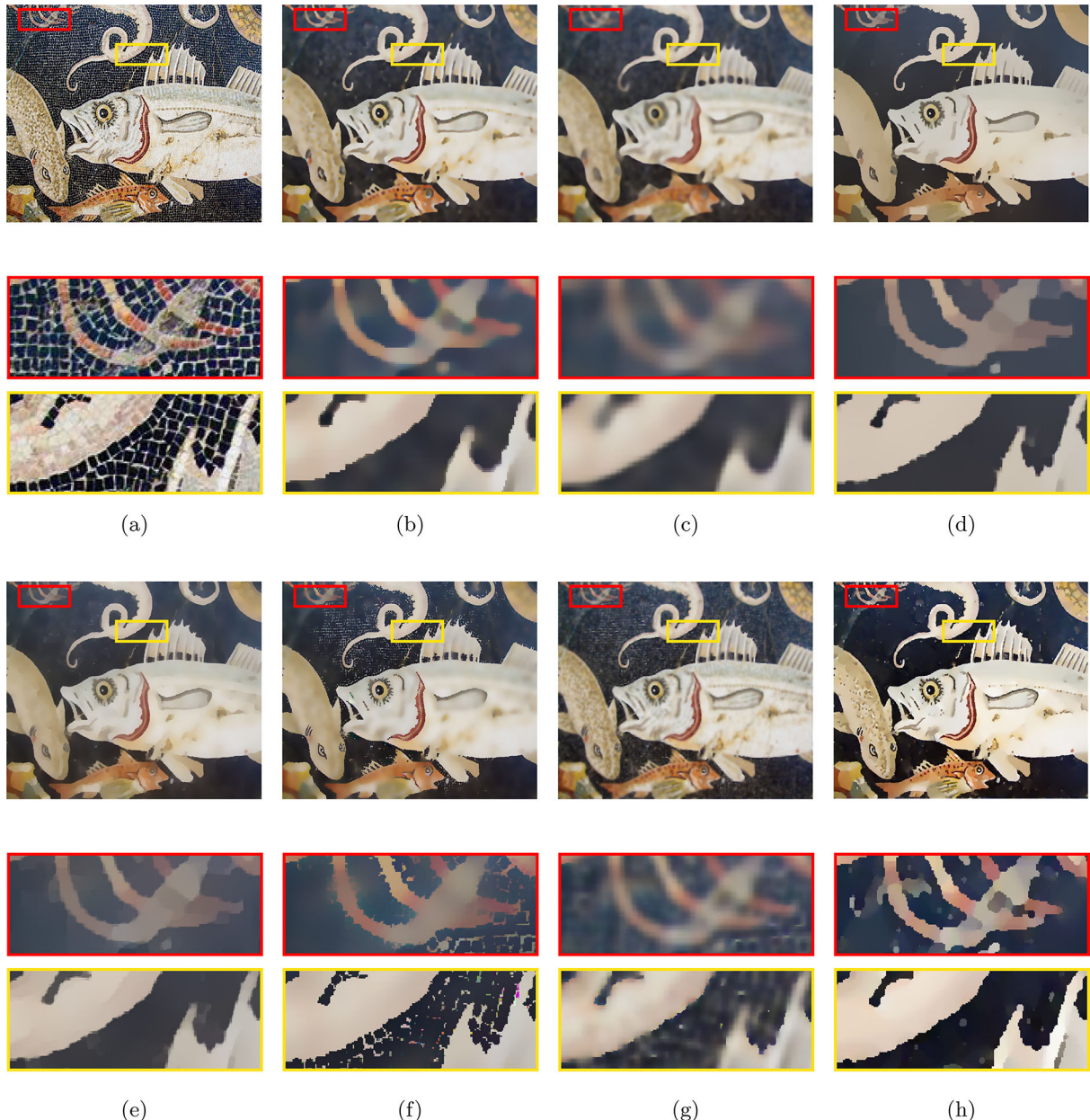


Fig. 10 Comparative results for part of the roman marine life mosaic image in pompeii: **a** Original image and some zoomed portions of it. Filter images obtained by applying **b** BTF, $k = 7, n_{itr} = 5$ [9], **c** SATF $ss = 4, sr = 0.05, st = 0.1, n_{itr} = 7, div = 30$ [19], **d**

RoG, $\lambda = 0.01, \sigma_1 = 2, \sigma_2 = 4, K = 4, dec = 2.0$ [7], **e** SATV, $\lambda = 1.25, n_{itr} = 19$ [38], **f** FABF $\rho_{smooth} = 5, \rho_{sharp} = 5$ [14], **g** ILS, $\lambda = 0.35, \gamma = 50/255, n_{itr} = 25$ [27], and **h** Proposed, $W = 31 \times 31, n_{itr} = 4$

preventing from over-sharpening and/or over-blurring artifacts/distortions.

5.2 Quantitative comparison

From the recent studies it was found that the classical non-subjective Image Quality Assessment (IQA) metrics like Peak Signal to Noise Ratio (PSNR), Signal to Noise Ratio (SNR) are not good enough for assessing the quality of

the filtered images, especially when they are generated by structure-preserving or texture filtering techniques [50]. The subjective reference IQA metrics such as Structural Similarity Index (SSIM) [47], Multi-scale SSIM (MSSIM), Mutual Information (MI) [43] and the subjective no-reference metrics like Perception Image Quality Evaluator (PIQE) [44] and Naturalness Image Quality Evaluator (NIQE) are more closer to human perception. For more details about these IQA metrics reader may refer to [43,44,47,50]. In order



Fig. 11 Comparative results for part of a roman still life mosaic image: **a** Original image and the filter images obtained by applying **b** BTF, $k = 9$, $n_{itr} = 7$ [9], **c** SATF $ss = 3$, $sr = 0.1$, $st = 0.1$, $n_{itr} = 7$, $div = 30$ [19], **d** RoG, $\lambda = 0.01$, $\sigma_1 = 1$, $\sigma_2 = 2$, $K = 4$, $dec = 2.0$ [7], **e** SATV, $\lambda = 2.5$ [38], **f** FABF $\rho_{smooth} = 2$, $\rho_{sharp} = 4$ [14], **g** ILS, $\lambda = 0.5$, $\gamma = 25/255$, $n_{itr} = 15$ [27], and **h** Proposed, $W = 7 \times 7$, $n_{itr} = 3$

to assess the effectiveness of the proposed technique in terms of both texture smoothing and structure preserving, a quantitative comparison is performed with help of three subjective reference IQA metrics SSIM, MSSIM, MI, and a subjective no-reference metric PIQE. Table 2 reports the values provided by those IQA metrics for different filtered



Fig. 12 Comparative results for a brick wall graffiti image: **a** Original image and the filter images obtained by applying **b** BTF, $k = 9$, $n_{itr} = 7$ [9], **c** SATF $ss = 7$, $sr = 0.1$, $st = 0.1$, $n_{itr} = 7$, $div = 30$ [19], **d** RoG, $\lambda = 0.01$, $\sigma_1 = 1$, $\sigma_2 = 2$, $K = 4$, $dec = 2.0$ [7], **e** SATV, $\lambda = 0.75$ [38], **f** FABF $\rho_{smooth} = 5$, $\rho_{sharp} = 5$ [14], **g** ILS, $\lambda = 0.75$, $\gamma = 50/255$, $n_{itr} = 25$ [27], and **h** Proposed, $W = 7 \times 7$, $n_{itr} = 7$

images. From this table, one can see that for the natural texture images, the proposed technique always provides better results than all six state-of-the-art methods considered for comparison. For the Lena image with artificial texture and noise, our method yields comparable results to the best literature method. Thus, by analysing the quantitative and the qualitative results we can conclude that the proposed technique outperforms the existing state-of-the-art techniques in terms of both, texture smoothing and structure preserving.

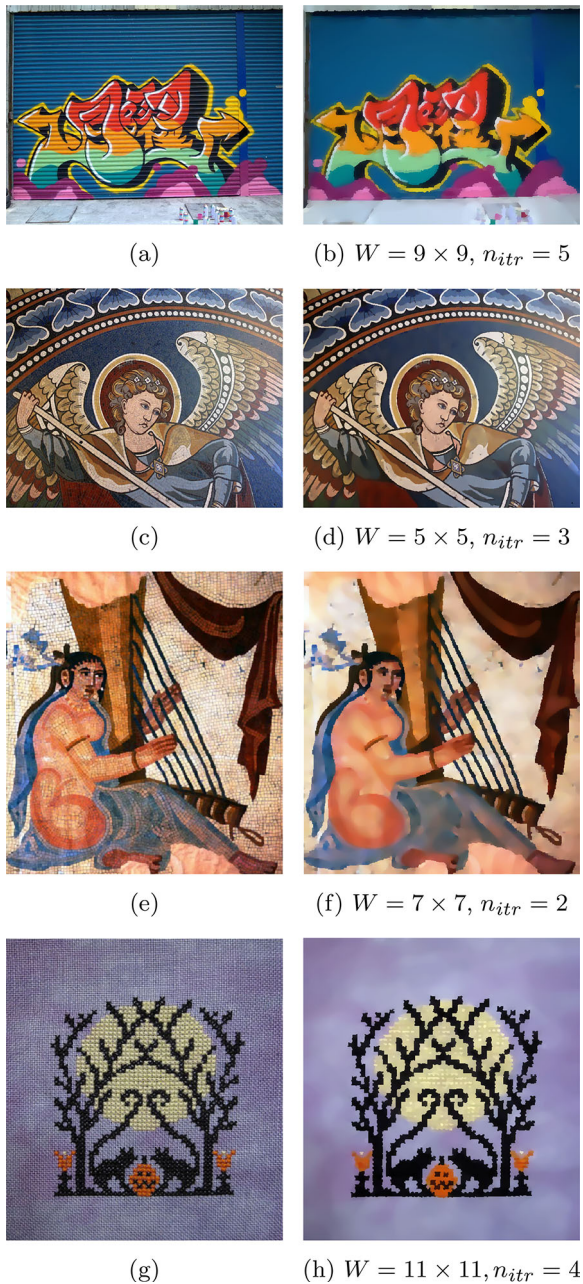


Fig. 13 **a, b, c, d** Original images, and **e, f, g, h** the filter images obtained by the proposed technique

5.3 Parameters setting and analysis

In order to take into account the neighbor pixels information, the proposed technique considers a few windows. The window W used to form the local histogram of the gradient image for computing the local skewness is one such parameter of the proposed technique. The optimum size of this window is dependent on the scale and size of the texels (single textural pattern) present in the input image. In the experiment the size of W is set manually by looking at the input image. The

square windows L_w and W_s of the proposed technique are the spatial parameters supplied as input to the median filter for filtering textural and structural-edge pixels, respectively. Since our technique increases the initial size of L_w in an adaptive manner, the size of the square window L_w should be small (can be taken from 3×3 to 11×11 depending on the size of the small structure to be preserved) and is not a critical parameter to set. In the experiment, the initial size of L_w is set to 3×3 for all the considered images. As for filtering structural-edge pixels, the window W_s is divided into two parts along with the edge alignment. The size of W_s should cover sufficient pixels to form two groups. If we fix the size of W_s very large, then there is a possibility of overlapping the textural and structural edges. Experimentally we found that the size of W_s between 5×5 to 11×11 provides satisfactory results for a wide variety of images. Note that the size of the square window W_s is not a critical parameter to set as our technique dynamically reshapes it before filtering. Taking its size smaller preserves more but smoothing needs more iterations. In the experiment the size of W_s is set to 7×7 for all the considered images. For morphological filtering, the proposed technique uses a small SE of size 3×3 . Table 3 shows the list of parameters of the proposed technique and their suggested values. From this table, one can see that the proposed technique has only critical parameter W . Figure 15 shows filter images and their corresponding values of different IQA metrics provided by the proposed technique by varying the size of the window W .

5.4 Computational performance analysis

The proposed technique has two important steps. First, it generates the edge-map, then based on the generated edge-map, adaptive median morpho-filtering produces the filter image. The edge-map generation followed by median morpho-filtering iteratively executed to generate the final filter image. The edge-map generation step has the complexity of $O(M \times N \times W)$, where $M \times N$ is the size of the image and W is the window for local gradient skewness calculation. The adaptive median morpho-filtering has the complexity of $O(M \times N \times W_s^a)$, where W_s^a is the adaptive window for filtering edge and non-edge pixels. So, the computational complexity of the proposed algorithm is $O(M \times N \times W')$, where $W' = \max\{W, W_s^a\}$.

The proposed technique and the available Matlab codes of the 6 state-of-the-art techniques used for comparison are executed on a 3.70 GHz Xeon(R)-8 Core(s) processor with 128 GB RAM. Table 4 shows the execution time (in seconds) of different techniques. From this table, one can see that although the proposed technique takes lesser time than the existing SATF technique and comparable time with BTF technique, but it takes significantly higher time than the RoG, SATV, FABF, and ILS techniques. Note that our current Mat-



Fig. 14 **a** Original Lena image and the image after adding artificial **b** textural grid and **c** Gaussian noise (mean=0, variance=0.01) to it. **d** The filter image of **c** obtained by applying the proposed technique with $W = 21 \times 21$, $n_{itr} = 4$

Table 2 The values of the IQA metrics SSIM, MSSIM, MI and PIQE obtained for the filter images generated by the different techniques

Images	Metrics	BTF	SATF	RoG	SATV	FABF	ILS	Proposed
	<i>SSIM</i>	0.43	0.41	0.42	0.42	0.44	0.42	0.48
Marine life	<i>MSSIM</i>	0.58	0.55	0.50	0.51	0.47	0.58	0.63
PIQE=20.18	<i>MI</i>	1.74	1.72	1.65	1.69	1.67	1.73	1.80
	<i>PIQE</i>	89.10	89.56	88.64	82.90	90.03	89.34	79.37
	<i>SSIM</i>	0.56	0.53	0.56	0.55	0.50	0.57	0.59
Still life	<i>MSSIM</i>	0.76	0.69	0.70	0.70	0.61	0.74	0.77
PIQE=34.63	<i>MI</i>	2.30	2.27	2.30	2.28	2.26	2.31	2.35
	<i>PIQE</i>	86.86	88.85	86.64	75.28	85.30	86.82	75.10
	<i>SSIM</i>	0.75	0.72	0.78	0.72	0.74	0.71	0.79
Graffiti	<i>MSSIM</i>	0.68	0.57	0.71	0.56	0.58	0.62	0.74
PIQE=27.43	<i>MI</i>	2.03	1.92	2.11	1.90	1.88	1.89	2.27
	<i>PIQE</i>	86.74	92.19	87.70	87.23	87.39	83.05	78.88
Lena original	<i>SSIM</i>	0.92	0.92	0.89	0.91	0.71	0.90	0.93
PIQE=17.65	<i>MSSIM</i>	0.87	0.87	0.71	0.79	0.44	0.78	0.87
(With grid&noise)	<i>MI</i>	2.69	2.67	2.44	2.51	1.75	2.03	2.07
PIQE=50.56	<i>PIQE</i>	91.43	93.23	92.50	79.73	83.44	100	79.67

The bold font indicates the best values of these IQA metrics

Table 3 List of parameters of the proposed technique and their suggested values

Parameters	Used for	Suggested range	Taken in experiment
W	Local gradients skewness calculation	5×5 to 41×41	Set manually
L_w	Filtering textural pixels	3×3 to 11×11	3×3
W_s	Filtering edge pixels	5×5 to 11×11	7×7
SE	Morphological operations	3×3 or 5×5	3×3
n_{itr}	No of iterations	1 to 10	Set manually

lab implementation is worked on a CPU environment and is not heavily optimized. It takes some time for skewness, adaptive windows, and median computation, which can be

greatly improved by parallel GPU implementation [15] and by using more clever sampling [18] and sorting algorithm (like counting sort [36]).

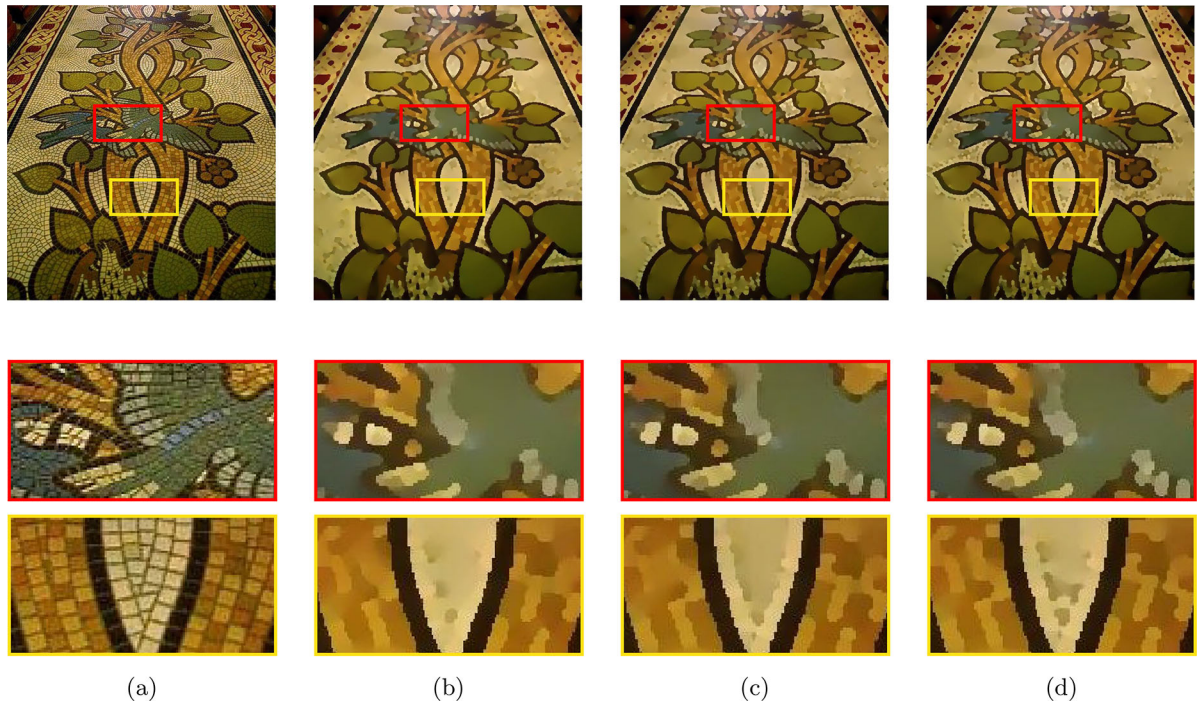


Fig. 15 **a** Original image of a mosaic floor ($\text{PIQE}=38.97$) and some zoomed portions of it. Filtered images obtained by the proposed technique after iteration 3 for **b** $W = 7 \times 7$ ($\text{SSIM}=0.75$,

$\text{MSSIM}=0.76, \text{MI}=2.27, \text{PIQE}=79.92$), **c** $W = 15 \times 15$ ($\text{SSIM}=0.75, \text{MSSIM}=0.77, \text{MI}=2.28, \text{PIQE}=78.34$, and **d** $W = 23 \times 23$ ($\text{SSIM}=0.76, \text{MSSIM}=0.77, \text{MI}=2.28, \text{PIQE}=78.50$))

Table 4 The execution time (in seconds) of the proposed and the state-of-the-art methods

Images	BTF	SATF	RoG	SATV	FABF	ILS	Proposed
Marine life	56.04	77.95	9.96	5.57	7.47	3.21	56.67
Still life	11.05	53.46	5.49	3.94	5.05	2.98	19.01
Graffiti	46.42	101.58	10.08	7.50	7.76	3.51	88.20

6 Conclusion

The main challenge for developing a robust structure-preserving filtering technique lies in the fact of handling varying scale textural patterns. In order to better handle varying scale textural patterns, in this paper we have proposed a semantic-aware structure-preserving filtering technique. Our technique defines a novel method to obtain an edge-aware adaptive window of dynamic shape for filtering each pixel by excluding its neighbor pixels belonging to different textural or structural regions. To this end, at first, a novel approach is proposed to generate the edge-map by analysing the skewness of global and local histograms of the morphological gradient. Then, using the generated edge-map a semantic-aware structure-preserving median morpho-filtering is designed by combining the output of median and morphological filters. The main contributions of this work are: (i) proposes a texture structure decomposition technique analysing the global and local morphological gradient distribution, and (ii) pro-

poses a combined median morpho-filtering for better texture smoothing while preserving the significant structures. Unlike most of the existing techniques, our filtering can achieve multiple conflicting goals, like identifying and removing texture, preserving structural edges, protecting easy-to-miss features such as corners, and preventing over-sharpening and/or over-blurring artifacts/distortions.

Although the proposed technique successfully works on a variety of images but our present implementation is not of real-time. Implementation of the proposed technique in real-time or near real-time and apply this technique to different image/video processing applications like semantic segmentation, object detection and classification etc would be an interesting extension of this work.

Funding This work is supported by Science and Engineering Research Board, Government of India, with Grant No. CRG/2020/003018.

Declarations

Conflict of interest The authors declare that they have no conflict of interest.

References

1. AlSaeed, D.H., Bouridane, A., ElZaart, A., Sammouda, R.: Two modified Otsu image segmentation methods based on lognormal and gamma distribution models. In: International Conference on Information Technology and e-Services (2012), IEEE, pp. 1–5
2. Annaby, M., Nehary, E.: Bilateral filters with adaptive generalized kernels generated via Riemann–Lebesgue theorem. *J. Signal Process. Syst.* **93**(11), 1301–1322 (2021)
3. Bao, L., Song, Y., Yang, Q., Yuan, H., Wang, G.: Tree filtering: efficient structure-preserving smoothing with a minimum spanning tree. *IEEE Trans. Image Process.* **23**(2), 555–569 (2013)
4. Ben Said, A., Hadjidj, R., Foufou, S.: Total variation for image denoising based on a novel smart edge detector: an application to medical images. *J. Math. Imaging Vis.* **61**(1), 106–121 (2019)
5. Berkovich, H., Malah, D., Barzohar, M.: Non-local means denoising using a content-based search region and dissimilarity kernel. In: 8th International Symposium on Image and Signal Processing and Analysis (ISPA) (2013), IEEE, pp. 10–15
6. Buades, A., Coll, B., Morel, J.: Image denoising methods: a new nonlocal principle. *SIAM Rev.* **52**(1), 113–147 (2010)
7. Cai, B., Xing, X., Xu, X.: Edge/structure preserving smoothing via relativity-of-Gaussian. In International Conference on Image Processing (ICIP) (2017), IEEE, pp. 250–254
8. Chan, L., Fu, G.: Structure-preserving image smoothing with semantic cues. *Vis. Comput.* **36**, 2017–2027 (2022)
9. Cho, H., Lee, H., Kang, H., Lee, S.: Bilateral texture filtering. *ACM Trans. Graph. (TOG)* **33**(4), 1–8 (2014)
10. Diamantaris, S., Alexis, K.: Modeling pixel intensities with log-normal distributions for background subtraction. In: International Conference on Imaging Systems and Techniques (IST) (2017), IEEE, pp. 1–6
11. Du, H., Jin, X., Willis, P.J.: Two-level joint local Laplacian texture filtering. *Vis. Comput.* **32**(12), 1537–1548 (2016)
12. Farbman, Z., Fattal, R., Lischinski, D., Szeliski, R.: Edge-preserving decompositions for multi-scale tone and detail manipulation. *ACM Trans. Graph. (TOG)* **27**(3), 1–10 (2008)
13. Gastal, E.S., Oliveira, M.M.: Domain transform for edge-aware image and video processing. *ACM Trans. Graph. (TOG)* **30**(4), 1–12 (2011)
14. Gavaskar, R.G., Chaudhury, K.N.: Fast adaptive bilateral filtering. *IEEE Trans. Image Process.* **28**(2), 779–790 (2019)
15. Green, O.: Efficient scalable median filtering using histogram-based operations. *IEEE Trans. Image Process.* **27**(5), 2217–2228 (2017)
16. Hays, J., Leordeanu, M., Efros, A.A., Liu, Y.: Discovering texture regularity as a higher-order correspondence problem. In: European Conference on Computer Vision. Springer, Berlin, pp. 522–535 (2006)
17. He, K., Sun, J., Tang, X.: Guided image filtering. *IEEE Trans. Pattern Anal. Mach. Intell.* **35**, 1397–1409 (2013)
18. Huang, T., Yang, G., Tang, G.: A fast two-dimensional median filtering algorithm. *IEEE Trans. Acoust. Speech Signal Process.* **27**(1), 13–18 (1979)
19. Jeon, J., Lee, H., Kang, H., Lee, S.: Scale-aware structure-preserving texture filtering. *Comput. Graph. Forum* **35**(7), 77–86 (2016)
20. Kang, X., Li, S., Benediktsson, J.A.: Spectral–spatial hyperspectral image classification with edge-preserving filtering. *IEEE Trans. Geosci. Remote Sens.* **52**(5), 2666–2677 (2013)
21. Karacan, L., Erdem, E., Erdem, A.: Structure-preserving image smoothing via region covariances. *ACM Trans. Graph. (TOG)* **32**(6), 1–11 (2013)
22. Lee, H., Jeon, J., Kim, J., Lee, S.: Structure-texture decomposition of images with interval gradient. In: Computer Graphics Forum, vol. 36, pp. 262–274. Wiley Online Library (2017)
23. Likforman-Sulem, L., Darbon, J., Smith, E.H.B.: Enhancement of historical printed document images by combining total variation regularization and non-local means filtering. *Image Vis. Comput.* **29**(5), 351–363 (2011)
24. Lin, T.H., Way, D.L., Shih, Z.C., Tai, W.K., Chang, C.C.: An efficient structure-aware bilateral texture filtering for image smoothing. In Computer Graphics Forum, vol. 35, pp. 57–66. Wiley Online Library (2016)
25. Liu, B., Lu, X.: Pointwise shape-adaptive texture filtering. In: IEEE International Conference on Multimedia and Expo (ICME), pp. 1–6 (2018)
26. Liu, C., Shao, H., Wu, M., Zhou, Y., Shao, Y., Wang, X.: Multi-scale inherent variation features-based texture filtering. *Vis. Comput.* **33**(6), 769–778 (2017)
27. Liu, W., Zhang, P., Huang, X., Yang, J., Shen, C., Reid, I.: Real-time image smoothing via iterative least squares. *ACM Trans. Graph. (TOG)* **39**(3), 1–24 (2020)
28. Liu, Y., Lin, W.C., Hays, J.: Near-regular texture analysis and manipulation. *ACM Trans. Graph. (TOG)* **23**(3), 368–376 (2004)
29. Liu, Y., Liu, G., Liu, H., Liu, C.: Structure-aware texture filtering based on local histogram operator. *IEEE Access* **8**, 43838–43849 (2020)
30. Ochotorena, C.N., Yamashita, Y.: Anisotropic guided filtering. *IEEE Trans. Image Process.* **29**, 1397–1412 (2019)
31. Paris, S., Hasinoff, S.W., Kautz, J.: Local Laplacian filters: edge-aware image processing with a Laplacian pyramid. *ACM Trans. Graph.* **30**(4), 68 (2011)
32. Perona, P., Malik, J.: Scale-space and edge detection using anisotropic diffusion. *IEEE Trans. Pattern Anal. Mach. Intell.* **12**(7), 629–639 (1990)
33. Rivest, J.F., Soille, P., Beucher, S.: Morphological gradients. *J. Electron. Imaging* **2**(4), 326–336 (1993)
34. Rudin, L.I., Osher, S., Fatemi, E.: Nonlinear total variation based noise removal algorithms. *Physica D: Nonlinear Phenomena* **60**(1–4), 259–268 (1992)
35. Ruhela, R., Gupta, B., Singh Lamba, S.: An efficient approach for texture smoothing by adaptive joint bilateral filtering. *Vis. Comput.* 1–15 (2022)
36. Saian, P.O.N.: Parallel counting sort: a modified of counting sort algorithm. *Int. J. Inf. Technol. Bus.* **1**(1), 10–15 (2018)
37. Serra, J.: *Image Analysis and Mathematical Morphology*. Academic Press Inc, New York (1983)
38. Song, J., Cho, H., Yoon, J., Yoon, S.M.: Structure adaptive total variation minimization-based image decomposition. *IEEE Trans. Circuits Syst. Video Technol.* **28**(9), 2164–2176 (2017)
39. Su, Z., Luo, X., Artusi, A.: A novel image decomposition approach and its applications. *Vis. Comput.* **29**(10), 1011–1023 (2013)
40. Sun, Y., Schaefer, S., Wang, W.: Image structure retrieval via L_0 minimization. *IEEE Trans. Vis. Comput. Graph.* **24**(7), 2129–2139 (2017)
41. Sun, Z., Liu, T., Li, J., Wang, Y., Gao, X.: Patch-based co-occurrence filter with fast adaptive kernel. *Signal Process.* **185**, 108089 (2021)
42. Tomasi, C., Manduchi, R.: Bilateral filtering for gray and color images. In: 6th International Conference on Computer Vision, IEEE, pp. 839–846 (1998)

43. Tsai, D.-Y., Matsuyama, E., Lee, Y.: A mutual information-based image quality metric for medical imaging systems. In: Medical Imaging, IntechOpen (2011)
44. Venkatanath, N., Praneeth, D., Bh, M.C., Channappayya, S.S., Medasani, S.S.: Blind image quality evaluation using perception based features. In: 2015 Twenty First National Conference on Communications (NCC), IEEE, pp. 1–6 (2015)
45. Wang, C., Xu, L., Liu, L.: Structure-texture image decomposition via non-convex total generalized variation and convolutional sparse coding. *Vis. Comput.* (2022)
46. Wang, H., Cao, J., Liu, X., Wang, J., Fan, T., Hu, J.: Least-squares images for edge-preserving smoothing. *Comput. Vis. Media* **1**(1), 27–35 (2015)
47. Wang, Z., Bovik, A.C., Sheikh, H.R., Simoncelli, E.P.: Image quality assessment: from error visibility to structural similarity. *IEEE Trans. Image Process.* **13**(4), 600–612 (2004)
48. Xu, L., Lu, C., Xu, Y., Jia, J.: Image smoothing via L_0 gradient minimization. *ACM Trans. Graph. (TOG)* **30**(6), 1–12 (2011)
49. Xu, L., Yan, Q., Xia, Y., Jia, J.: Structure extraction from texture via relative total variation. *ACM Trans. Graph. (TOG)* **31**(6), 1–10 (2012)
50. Xu, P., Wang, W.: Improved bilateral texture filtering with edge-aware measurement. *IEEE Trans. Image Process.* **27**(7), 3621–3630 (2018)
51. Xu, P., Wang, W.: Structure-aware window optimization for texture filtering. *IEEE Trans. Image Process.* **28**(9), 4354–4363 (2019)
52. Yang, G.Z., Burger, P., Firmin, D.N., Underwood, S.: Structure adaptive anisotropic image filtering. *Image Vis. Comput.* **14**(2), 135–145 (1996)
53. Yang, Q.: Semantic filtering. In: Proceedings of the IEEE conference on computer vision and pattern recognition (06 2016), pp. 4517–4526
54. Ye, W., Ma, K.K.: Semantic image content filtering via edge-preserving scale-aware filter. In: IEEE International Conference on Image Process. (ICIP), pp. 2443–2447 (2017)
55. Yin, H., Gong, Y., Qiu, G.: Side window guided filtering. *Signal Process.* **165**, 315–330 (2019)
56. Zhang, B., Allebach, J.P.: Adaptive bilateral filter for sharpness enhancement and noise removal. *IEEE Trans. Image Process.* **17**(5), 664–678 (2008)
57. Zhang, G., Wang, J., Zhang, X., Fei, H., Tu, B.: Adaptive total variation-based spectral–spatial feature extraction of hyperspectral image. *J. Vis. Commun. Image Represent.* **56**, 150–159 (2018)
58. Zhao, H., Jiang, L., Jin, X., Du, H., Li, X.: Constant time texture filtering. *Vis. Comput.* **34**(1), 83–92 (2018)
59. Zhou, P.-C., Xue, Y., Xue, M.-G.: Adaptive side window joint bilateral filter. *Vis. Comput.* 1–23 (2022)
60. Zhu, L., Hu, X., Fu, C.W., Qin, J., Heng, P.A.: Saliency-aware texture smoothing. *IEEE Trans. Vis. Comput. Graph.* **26**(7), 2471–2484 (2018)

Publisher's Note Springer Nature remains neutral with regard to jurisdictional claims in published maps and institutional affiliations.

Springer Nature or its licensor (e.g. a society or other partner) holds exclusive rights to this article under a publishing agreement with the author(s) or other rightsholder(s); author self-archiving of the accepted manuscript version of this article is solely governed by the terms of such publishing agreement and applicable law.

Kunal Pradhan received M.Tech. degree from Kalyani Government Engineering College, India in 2015. He is currently working towards the Ph.D. degree at the Department of Computer Science and Engineering, Tezpur University, India. His research interests include morphological image processing, texture structure image decomposition and processing.

Swarnajyoti Patra is an assistant professor at the Department of Computer Science and Engineering, Tezpur University, India. He received his Ph.D. degree in engineering from Jadavpur University, India, in 2009. His research interests include feature extraction, feature selection, mathematical morphology, pattern recognition, and image processing.